Coastal Engineering 152 (2019) 103515

Contents lists available at ScienceDirect

Coastal Engineering

journal homepage: www.elsevier.com/locate/coastaleng

Scour development around a jacket structure in combined waves and current conditions compared to monopile foundations

M. Welzel*, A. Schendel, A. Hildebrandt, T. Schlurmann

Ludwig-Franzius-Institute for Hydraulic, Estuarine and Coastal Engineering, Leibniz Universität Hannover, Nienburger Str. 4, 30167, Hannover, Germany

ARTICLE INFO

Keywords:
Scour
Jacket
Hydrodynamic transparent
Wave-current interaction
Sediment transport
Laboratory tests

ABSTRACT

This paper presents the results of an experimental study on the scour development of a hydraulic-transparent offshore foundation exposed to combined waves and current. Irregular waves propagating perpendicular to a current were simulated in a wave-current basin. The physical model tests were conducted in a length scale of 1:30 while measurements of the scour development over time were achieved by echo sounding devices placed at several locations at the upstream and downstream side of the jacket structure. Insights were gained on the scour development and time scale of the scouring process around a complex jacket structure for different wave-current conditions. The results were presented with respect to the Keulegan-Carpenter KC number and the relative wave-current velocity. Wave conditions were adjusted so that KC numbers between 6.7 and 23.4 could be tested in a systematic wave-current test program with tests reaching from wave dominated conditions up to current dominated conditions. Measured scour depths were critically assessed by an extrapolation to expected equilibrium scour depths. With respect to the current flow direction, the experiments showed generally larger scour depths at the upstream side and lower scour depths on the downstream side for each pile of the jacket structure. The development of global scour around the structure intensified with increasing relative wave-current velocity. As a result, a practical formulation is proposed for the reliable prediction of local scour depths around a jacket foundation in combined wave-current conditions. Finally, dimensionless time scales and observed as well as predicted scour depths are compared to values for the scour development around monopiles.

1. Introduction and motivation

In the search for sustainable renewable energy forms, offshore wind parks within coastal areas are expanding to meet rising energy demands. Considering the lack of space in near shore coastal zones, upcoming wind parks build at larger water depths can provide a significant share of energy (Sun et al., 2012). In contrast to onshore installations, the emergence of scour around foundations needs to be taken into account in the design process of offshore wind structures. Given the uncertainties inherent to reliably assess the presence and extent of scouring phenomena around more complex structures, various practical options exist to counteract structural-induced erosion processes at marine infrastructures. Due to a lack of knowledge about scour around complex, hydrodynamic transparent jacket-type foundations in particular, offshore wind energy converters (OWEC) are often designed following an approach for monopiles (Bolle et al., 2012). Consequently, this can lead to a conservative and uneconomic design (Stahlmann and Schlurmann, 2010) or may lead to an uncertain prediction of local and global scour depth (Rudolph et al., 2004).

Fundamental knowledge on scour processes and extent due to waves and currents preliminary exists for cylindrical structures. Yet, those insights are regularly taken as a basis for scour prediction and the design of scour protection systems around more complex offshore foundations. Scour development around piles in steady currents has been investigated extensively, particularly with respect to the scour development at bridge piers in uni-directional currents (e.g., Hjorth, 1975; Breusers et al., 1977; Raudkivi, 1986; Sumer et al., 1992a; Melville and Coleman, 2000; Sheppard et al., 2004; Sheppard and Miller, 2006). While the scouring process in currents is mainly induced by the horseshoe vortex, scour processes in waves have been observed to be more affected by vortex shedding at the lee side of the pile (Kobayashi and Oda, 1994; Sumer et al., 1992b, 1993, 1997, 2002), particularly for small Keulegan-Carpenter (KC) numbers. In comprehensive laboratory tests, Sumer and Fredsøe (2001) compared the scour development around piles with different diameters subjected to combined current and irregular waves. The scour depth was found to be a function of $U_{cw} = U_c/(U_c + U_m)$, which represents the ratio of undisturbed current U_c to wave generated flow velocity U_m. For values of $U_{cw} > 0.5$, the scour

* Corresponding author.
E-mail address: welzel@lufi.uni-hannover.de (M. Welzel).

https://doi.org/10.1016/j.coastaleng.2019.103515
Received 22 December 2018; Received in revised form 31 March 2019; Accepted 15 June 2019
Available online 18 June 2019

development becomes current dominated so that scour depths approach values obtained in current only conditions for values of U_{cw} larger than about 0.7. For low KC numbers it was found that a slight superimposed current causes the flow to form a stable horseshoe vortex, leading to an increase of wave induced scour depth. Based on these findings, Sumer and Fredsøe (2002) derived an empirically-driven prediction approach for combined wave and current conditions. In addition, Rudolph and Bos (2006) performed laboratory tests on the scour development at monopiles under combined waves and current conditions in low KC-numbers. The general backfilling mechanism and timescale in case of combined waves and current conditions was investigated by Sumer et al. (2013). Qi and Gao (2014) carried out physical model tests on the scour development in waves and current conditions with small KC numbers and included the assessment of the influence of pore pressure on the scour development. Zanke et al. (2011) developed a unifying empirically-based prediction approach by introducing a new transition function between the wave and current generated scour at singular piles.

To the authors knowledge, only few studies have been conducted regarding the scour development at jacket-type structures in waves and current conditions. Based on field measurements by multi-beam echo sounder, Bolle et al. (2012) analysed scour depths at jacket structures placed in the wind farm Thornton bank in the southern North Sea. The jacket structures at Thornton bank were installed following a so-called pre-piling attempt (D = approx. 2 m) with a distance between the pile centres of 18 m and a distance between the nodes and the sea bed of 2.5–5.0 m. The stick-up height of the four piles was about 1.5 m above the original sea bed. The authors found an average scour depth of S/D = 0.65 and a maximum scour depth of S/D = 1.2 only 2.5 months after the pre-pilling but before the installation of the jacket structures. Six months after the jacket installation, mean scour depths of different structures increased to values of S/D = 1.35. The scour depth estimation required for the design process of the jacket structures was based on existing formulas for local scour around monopiles and on investigations on the effect of pile groups on global scour (Breusers, 1972; Hirai and Kuruta, 1982; Sumer and Fredsøe, 2002). A comparison between estimated and measured scour depths revealed significant differences, and thus, emphasised the importance of continuous monitoring and further investigations.

Chen et al. (2014) carried out physical model tests with a jacket-type foundation for conditions around the coast of Taiwan, characterised by tidal currents and perpendicular approaching waves. Chen et al. simulated water depths of 12–16 m, wave heights of 2.5–6.8 m with wave periods of up to 11.7 s in a model scale of 1:36. Without having the exact geometrical dimensions of the structure, the distance between the main piles had to be estimated to be approximately 14 m. Compared to this structural footprint, the diameter (D = 2.08 m) of the four main piles was proportionally large, while the near bed braces were comparable thin (≈0.5 m). As a result, the influence due to flow obstruction and, thus, structure-induced streamline contraction and consequently near bed turbulence was less pronounced than for the structure analysed in Rudolph et al. (2004). Consequently, local scour depths of S/D = 0.2–1.3 were measured under combined waves and tidal current conditions by Chen et al. (2014).

Rudolph et al. (2004) analysed the scour development around a wellhead and a production platform in the southern North Sea, located at block L9 in front of the coast of the Netherlands, by using several field measurements. The jacket structures were installed in moderate water depths of h = 25 m. The wellhead platform was based on a jacket with four main piles with spacings of 20 m and 17 m and a diameter of D_1= 1.1 m. The jacket of the production platform consisted of six legs (D_2= 1.5 m), which had spacings of 16 m and 20 m, respectively. Both jackets were founded via additional post piles (of = 1,2 m and $D_{2,post}$ = 1,5 m) and had horizontal (approx. 0.65 m) and diagonal near bed braces (approx. 0.55 m). The authors found global scour around the structures with an extend of about 50 m (40 times the pile diameter) and local scour depths of up to 5 m ($S/D > 3$). A comparison to well-known scour prediction formulas for single piles revealed that scour depths are underestimated by a factor of 3–4. The authors explained the poor performance of the prediction approaches with the disturbing effect of the jacket structure on the flow close to the seabed. Rudolph et al. (2004) also stated that comparable scour depths were observed at similar jacket structures in the North Sea, indicating that the shown measurements depict no exception.

The scour process is caused by a complex vortex system around the foundation structure, consisting of the horseshoe vortex, a combined downflow at the front of the structure, vortex shedding at the back side as well as a contraction of the flow at the sides (Sumer and Fredsøe, 2001). The process varies with the shape of the foundation structure and consequently with the contraction of streamlines. Hence, the knowledge about scour development at piles cannot be directly transferred to more complex structures. In case of jacket-type foundations, the additional braces near the seabed cause the flow to contract, leasing to increased flow velocities and bed shear stresses. Moreover, additional vortices on the lee side of the braces might be introduced, further increasing the erosive potential of the flow on the seabed. The distance, angle and diameter of the braces, the general blockage effect (i.e. post pile foundations, Rudolph et al., 2004) as well as the ratio of the overall extent of the structure to the diameter of the main pile depict additional influence factors for the scour development.

The literature review reveals that unresolved questions regarding the scour development at jacket structures, in particular its progression over time and equilibrium scour depths for a wide range of KC and U_{CW} values, remain. In addition, the structural influence on the scour development, i.e. the angle, diameter and distance of the braces to the sea bed as well as the blockage effect on the scour development and their contribution to the overall scour depth still need to be investigated in more depth. The global and local erosion and deposition processes in the vicinity of a jacket structure and the controlling boundary conditions of global scour depth and extents. The analysis of flow processes as well as implications of waves superimposed on currents in different directions on the scour development. Furthermore, a direct comparison and analysis of differences between the scour development around jacket structures and monopiles might provide useful information to improve the scour estimation at jacket structures for design purposes.

In view of this situation, novel hydraulic model tests were carried out in the 3D wave and current basin of the Ludwig-Franzius-Institute to perform a systematic investigation and to yield a better understanding of the scouring processes around a jacket-type offshore structure under combined waves and current. The objectives of this study include:

1. The systematic investigation of the scour development over time in combined waves and current conditions at different locations at the front and back side of the jacket.
2. The definition of equilibrium scour depths in combined waves and current conditions for a wide range of Ucw and KC values.
3. The analysis of the related rate and time scale of the scour development.
4. To improve the scour prediction for jacket structures in marine conditions by comparing scour depths and time scales to that at monopiles.

2. Experimental setup

The experiments were carried out in the 3D wave and current basin of the Ludwig-Franzius-Institute, Leibniz Universität Hannover, Germany. The basin has a length of 40 m, a width of 24 m and a maximum water depth of about 1 m (see Fig. 1). The sediment pit in the middle of the basin has a length of 8 m, a width of 6.6 m and provides an additional depth of 1.2 m. A sediment trap at the downstream side of the sediment pit (with respect to the current direction) was installed to

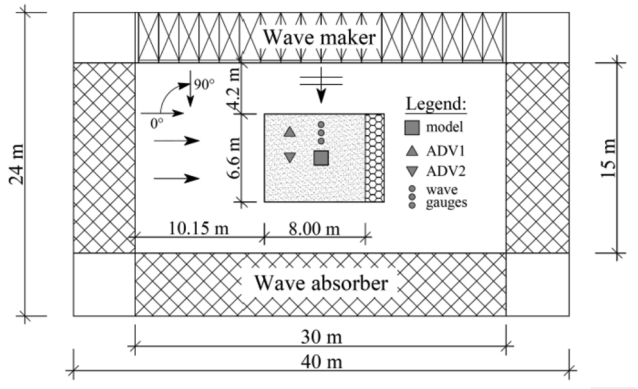

Fig. 1. Test setup in the wave-current basin, plan view, current is coming from left to right (0°), waves propagate towards 90°.

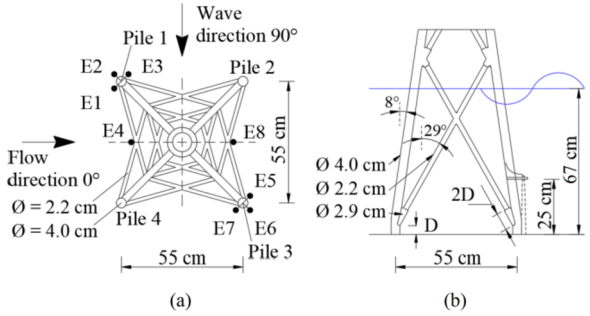

Fig. 2. Schematic view of the jacket model (a) schematic plan view of the positioned echo sounders, (b) schematic side view of the model with dimensions, diameters including the URS mounting, D = 4 cm.

prevent large sediment transport as bed load into the pump sump. Wave reflections are reduced by an integrated active and passive wave absorption system. As displayed in Fig. 2, the water level of 0.67 m (corresponds to a prototype water depth of 20 m, assuming a model length scale of 1:30) was kept constant during the model tests. The wavemaker consists of 72 individual wave paddles, allowing a generation of regular and irregular waves in variable wave angles. The experiments were conducted with incident waves propagating in the direction of 90° only, which is perpendicular to the current coming from 0° (see Fig. 1). A wave angle of 90° was chosen to ensure a better comparability with the studies of Schendel (2018) and Sumer and Fredsøe (2001). The current was generated by a pump system consisting of four pumps with a combined maximum flow capacity of 5 m^3/s, ensuring a depth-averaged mean flow velocity of up to 0.5 m/s for a water depth of 0.6 m.

A jacket-type platform, which was 3D printed, was used as foundation structure in the model tests. To obtain a smooth surface roughness, the model was sanded down, and painted with filler and lacquer in several layers. The piles below the lowest nodes, which were connected with the basin bottom, were made out of aluminium, providing a smooth surface. The jacket structure had a quadratic footprint with a width of 0.55 m. While the main piles, with a diameter of 4 cm each, were inclined 8° inwards and the diagonal braces were tilted 29° inwards (Fig. 2). The physical model was created to simulate a generic jacket-type shape without additional post piles and mud-mats. The model was constructed and installed so that the bottom of the lowest node was located at one pile diameter D (with D = 4 cm) above the sediment bed. As a result, a significant influence of the structure on the near bed flow was expected. The model was positioned in the centre of the sediment pit and securely tightened to the flume bottom. It was not rotated during the experiments, so that only one orientation of the jacket structure with respect to the current and wave direction was investigated. Sand with a median diameter of d_{50} = 0.19 mm, a density of ρ_s = 2.65 g/cm^3 and a geometric standard deviation $\sigma_s = \sqrt{(d84/d16)} = 1.4$ was used as sediment. To assure a good compaction and to reduce entrapped air, the sand was installed in wet condition (water level of a few millimetres) and levelled with aluminium bars. A settlement of the sediment was not observed after 16 h of waiting and several preliminary tests under different wave and current conditions. Additionally, glued gravel mats (gravel of 16–32 mm, width = 40 cm in current and 30 cm in wave direction) were installed at the inner edge of the sediment pit, with the purpose to mitigate edge scour. Compared to pre-tests without roughness elements, a significant reduction of the size and extension of the edge scour was observed. However, this assessment is based on visual observation as no measurements of the edge scour depth were conducted.

An array consisting of three ultrasonic wave gauges (ULS HF 58 by General Acoustics), measuring with a frequency of 200 Hz, was installed along a line between wavemaker and jacket structure. The wave gauge spacing was matched according to the wave lengths by using the principles of reflection analysis of Mansard and Funke (1980). Hereby, the middle wave gauge remained at a constant distance of 2 m from the centre of the model. The reflection coefficient was determined for every test with values between 0.34 and 0.38 for tests conducted with a significant wave height of H_s = 0.147, as well as values between 0.23 and 0.24 for H_s = 0.158 and 0.25–0.29 for tests related to H_s = 0.165. Wave and current induced flow velocities were measured by means of two Acoustic Doppler Velocimeter (ADV) (Vectrino+, Nortek AS, Norway). One was placed in line with the wave gauge array (ADV1), the other (ADV2) was positioned 2.5 m upstream (in current direction) from the jacket, see Fig. 1. Both ADV have been installed vertically (looking down) at a distance of 10 cm (2.5D) above the sediment bed, with their x-axis pointing in current direction. Measurements closer to the bed were not possible due to ripple migration and a minimum distance required for a good signal quality of the ADV.

Preliminary tests have been carried out to measure the horizontal, undisturbed current velocity 10 cm above the sediment bed, in the following referred to as U_c. Additionally, vertical profiles of streamwise flow velocity were collected to determine the undisturbed, depth averaged current velocity $\bar{U}$, at the location of ADV2. The undisturbed orbital velocities U_m were also measured during previously conducted tests with ADV1 placed 10 cm above the sand bed.

Measurements of the scour development over time around the complex structure were enabled by eight small echo sounding devices E1-E8 (Ultrasonic Ranging System - URS, Seatek) with a diameter of 1 cm each, placed at different positions around the jacket structure (Fig. 2). A similar system for scour depth measurements was used by McGovern et al. (2014). The echo sounders were mounted on the jacket in a distance of 1 cm next to the piles and were measuring the scour depth with a sampling frequency of 1 Hz. The URS measured the scour depth with a vertical resolution of 1 mm, and a half beam angle of 0.9°. The closest range of the URS is 3.5 cm and the furthest range 110 cm from the bottom. All sensors were equidistantly placed 25 cm (≈6 D, for smooth bed reference conditions) above the sea bed in order to ensure a rather small signal footprint of 2 cm in diameter to gain a narrow signal feedback from the eroded sea bed, but also to abate the intrusiveness of the sensor in regard of an unforced flow field disturbance with respect to the scouring process. Calibration tests regarding the accuracy of the URS were conducted under clear water and live bed conditions on a flat and sloped sea bed inside a scour hole, which confirmed a vertical accuracy of 1–2 mm. However, the calibration tests revealed that uncertainties stemming from large amounts of suspended sediment can interfere with the acoustic signal of the URS. Adjustments with respect to density, water temperature and threshold voltage in combination with reference measurements in calm conditions (see chapter 2.1) as well as different signal filters were considered to ensure a consistent accuracy of scour measurements. In the present setup, 6 URS echo sounders were positioned around 2 main piles of the

jacket structure (Fig. 2), of which one (pile 1) is located at the upstream and the other (pile 3) at the downstream side of the jacket with respect to the current flow direction. The echo sounders were positioned following the assumption that the maximum bed shear stress amplification around a circular pile can be generally expected to be located at approx. 45° to the direction of approaching flow for steady flow as well as waves only conditions (Hjorth, 1975; Baykal et al., 2017). However, during the tests, an increased scour depth has emerged under the braces. Unfortunately, a continuous measurement at this location was not possible as the URS signal would have been blocked by the structure itself. However, to provide additional insights in the progression of global scour induced by the structure, two echo sounder (E4 and E8 in Fig. 2) were also placed between the upstream and downstream piles, respectively.

2.1. Experimental procedure and test conditions

Prior to each test the sand bed was levelled to avoid influences due to sand bed irregularities and ripples. Subsequently, the water was carefully filled in the wave basin overnight. Irregular waves (JONSWAP spectra with a peak enhancement factor $\gamma = 3.3$, and spectral width parameters $\sigma_a = 0.07$ and $\sigma_b = 0.09$) were adopted for all tests as a realistic representation of offshore North Sea conditions. To reduce the influence of wave reflection over time as well as to enable additional scour depth reference measurements, the generated wave spectra were limited to approx. 650 waves. After each spectrum, a break of about 10 min was conducted, in which the current was shut down gradually and waves were stopped in a way that the last wave was generated at the exact time the current induced flow velocity fell under its critical value. This ensured that no single exposure due to waves or current contributes to the scour development. During each break, additional reference measurements of the scour depth were carried out under clear water conditions with the URS. A number of 650 waves was chosen to provide a sound basis for a meaningful distribution of waves within the random wave spectrum, as well as to keep the number of breaks within each test limited. The spectra were then repeated up to 10 times, until the scour process attained the equilibrium stage or a maximum amount of 6 500 waves were applied. Available studies related to scour around OWEC's due to combined waves and current often feature test durations in a range of 1–3 h (e.g. Raaijmakers and Rudolph, 2008; Petersen et al., 2012; Chen et al., 2014; Qi and Gao, 2014). As in some of those studies the equilibrium scour depth was not reached, a maximum number of 6 500 waves was selected for the tests presented herein, representing test durations between 3.7 and 8.3 h, to enable the scour process to reach its equilibrium state. The test procedure used in the combined waves and current tests can be summarized as follows:

1. Smoothing the sand bed and filling the basin.
2. Run the desired wave spectrum combined with the smallest design velocity U_c until the scour process has reached the equilibrium stage or a maximum number of 6 500 waves was applied.
3. Increase the current velocity to the next larger velocity value and repeat step 2.
4. Increase the current velocity to the highest velocity, repeat step 2.
5. Emptying the wave basin and draining the sand pit.

The physical model tests with waves only conditions followed the same procedure. After smoothing the sand level, the smallest wave spectrum was generated. Afterwards, the wave spectrum was increased, and the previous steps were repeated. Test 13 (see Table 1) was conducted separately under current only conditions following the described procedure. Wave parameters and current flow velocities were selected to cover a wide range of values for the KC number, U_{cw} and the Shields parameter θ, which are essential governing parameters effecting the scouring process in combined wave and current conditions. The maximum value of the undisturbed orbital velocity U_m can be calculated

Table 1
Measured values/Test conditions (waves are propagating in 90° to the current), with D = 4 cm, a water depth of 0.67 m, echo sounder E1-E3 relating to Pile 1 (upstream) as well as echo sounder E5-E7 relating to Pile 3 (downstream), see Fig. 2.

Test	H_s	T_p	Maximum bed orbital velocity U_m	Depth averaged current velocity $\bar{U}$	Current velocity 10 cm above bed U_c	Keulegan Carpenter number KC	$U_C/(U_C + U_m) = U_{cw}$	Shields Parameter θ	Pile 1 Nondimen-sional Timescale T^*	Pile 3 Nondimen-sional Timescale T^*	Pile 1 S_{end}/D	Pile 3 S_{end}/D	** Upstream side E4 S_{end}/D	** Downstream side E8 S_{end}/D	Test duration
	(m)	(s)	(cm/s)	(m/s)	(cm/s)	[−]	[−]	[−]	[−]	[−]	[−]	[−]	[−]	[−]	(min)
01	0.147	2.0	13.3	–	–	6.7	0	0.066	16.33	7.88	0.320	0.196	0.017	−0.020	220
02	0.158	3.4	17.5	–	–	14.9	0	0.075	0.70	4.79	0.442	0.339	−0.208	−0.081	380
03	0.165	4.5	20.8	–	–	23.4	0	0.080	2.70	16.04	0.788	0.659	−0.648	−0.435	500
04	0.147	2.0	13.3	11.4	10.1	6.7	0.43	0.067	34.63	27.19	0.464*	0.271*	0.030	−0.092	216
05	0.147	2.0	13.3	24.3	22.5	6.7	0.63	0.078	10.11	10.23	0.863	0.708	0.181	0.090	225
06	0.147	2.0	13.3	41.7	38.8	6.7	0.75	0.123	7.32	12.70	1.502	1.133*	0.254	0.361	221
07	0.158	3.4	17.5	11.4	10.1	14.9	0.37	0.076	21.71	20.31	0.735	0.622	−0.142	−0.159	383
08	0.158	3.4	17.5	24.3	22.5	14.9	0.56	0.087	16.69	17.08	1.205	1.038	0.305	0.253	391
09	0.158	3.4	17.5	41.7	38.8	14.9	0.69	0.131	14.83	24.14	1.784	2.035*	0.524	1.187	388
10	0.165	4.5	20.8	11.4	10.1	23.4	0.33	0.085	28.31	19.88	0.902	0.759	0.308	−0.133	500
11	0.165	4.5	20.8	24.3	22.5	23.4	0.52	0.096	12.74	21.41	1.253	1.189	0.435	0.213	498
12	0.165	4.5	20.8	41.7	38.8	23.4	0.65	0.138	28.21	35.36	1.696	2.140*	0.580	1.097	504
13	–	–	–	41.7	38.8	–	1.0	0.084	20.76	32.27	1.637*	1.354*	0.235	0.467	420

* S_{end} is smaller than 90% of the extrapolated equilibrium scour depth, which is used to assess the equilibrium stage of the scour development curve of each test, see 3.2.
** Streamwise sides of the jacket in current direction, see Fig. 2.

by:

$$U_m = \sqrt{2}\, U_{rms} \tag{1}$$

in which U_{rms} is defined as the root-mean-square (RMS) value of the orbital velocity U at the bed in direction of the waves. The root-mean-square velocity U_{rms} can be obtained by integration of the velocity frequency spectrum over all frequencies:

$$U_{rms}{}^2 = \int_0^\infty S(f)df \tag{2}$$

in which $S(f)$ is the power spectrum of U, which is corresponding to the wave component, and with f as the frequency.

As suggested by Sumer and Fredsøe (2001), the Keulegan-Carpenter number is defined as $KC = U_m T_p/D$, in which T_p is the peak wave period. The Shields parameter is based on the orbital velocity U_m and the current velocity U_c and was calculated based on the bed shear stress approach of Soulsby and Clarke (2005). The test program consisted of three different wave spectra with maximum orbital flow velocities between U_m = 13.3 and 20.8 cm/s, which were combined with three different current flow velocities U_c ranging from 10.1 cm/s to 38.8 cm/s. The KC numbers varied from $6.7 < KC < 23.4$ while U_{cw} ranged from $0 < U_{cw} < 1$. The critical Shields parameter of the sediment, $\theta_{cr} = 0.049$, was calculated according to Soulsby (1997):

$$\theta_{cr} = \frac{0.3}{1 + 1.2D^*} + 0.055[1 - \exp(-0.02D^*)] \tag{3}$$

in which $D^* = d_{50}[(s-1)g/v^2]^{1/3}$ is the dimensionless grain size, $s$is the specific density of the sand, g gravitational acceleration and v the viscosity of water. As shown in Table 1 the test series have been conducted for live bed conditions only. Note that test 1, 2 and 3 as well as test 13 were carried out to showcase scouring experiments in wave only and current only environments in order to complement the test condition matrix and yield comparative understanding to the combined waves and currents experiments. The final scour depth S_{end}/D depicted in Table 1 is defined as the mean value of scour depths measured during the last 25% of each test. The duration was chosen depending on the fluctuation period of the signal. It was found that a mean value of the last 25% is representing the measured scour depth more appropriate as e.g. the maximum scour depth, or a mean value of a shorter signal which tend to vary more for the present tests. Nevertheless, it has to be pointed out that in other tests, in which the scour depth was steadily increasing until the end, using an average value probably leads to a slight underestimation of final scour depths.

3. Results and discussion

3.1. Flow and scouring mechanisms

In the present study the scouring process around a foundation structure under combined waves and current was investigated. For the scour development around a jacket structure, it is reasonable to assume that its main mechanisms are related to the local flow acceleration around the piles, which in turn lead to a mobilization and consequently to a transport of sediment downstream (in current direction). Similarly, it can also be presumed that structural elements like near bed diagonal braces cause additional vortex shedding and streamline contraction compared to a single pile, also potentially increasing the sediment mobilization around the jacket structure. Furthermore, the downstream located pile (as well as downstream located sediment areas) might interfere with the wake dynamics of the upstream located piles and braces, similar to two circular cylinders in a tandem configuration (Mubeen, 2008; Sumner, 2010). Considering these potential influences of the structure on the flow, a significantly different scour development than that around a single pile can thus be expected. However, jacket type foundations can vary in certain structural parameters. For example, in case of a jacket structure with a large distance between the

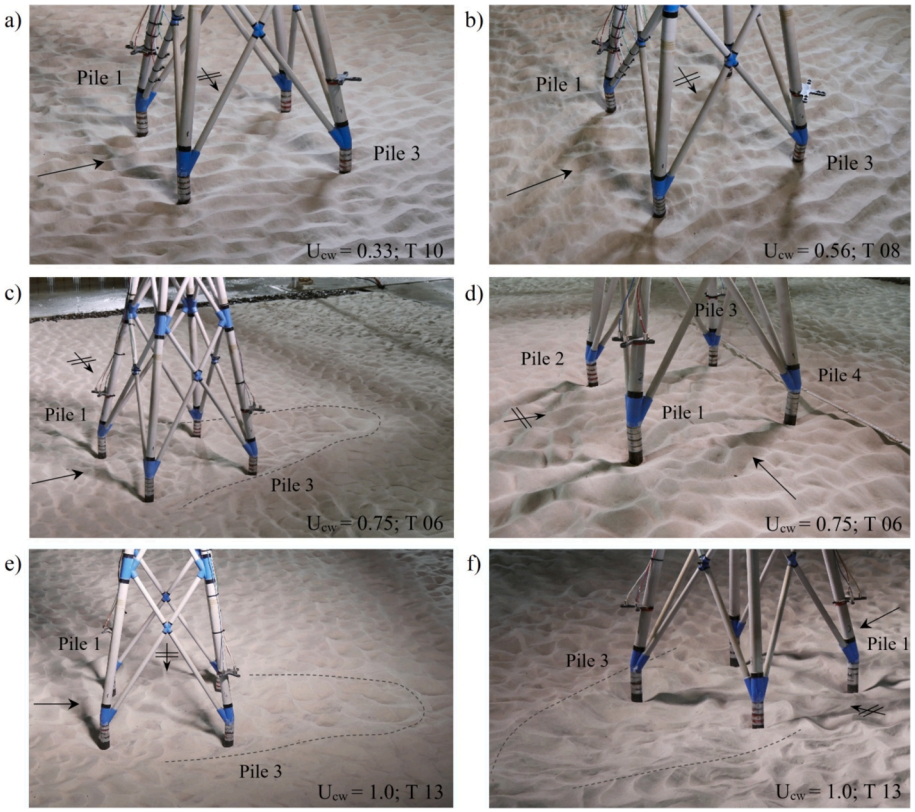

Fig. 3. Scour pattern for wave dominated up to steady current conditions (U_{cw} = 0.33–1.0), exemplary presented with photos of the bed topography after test 6, 8, 10 and 13. The dashed line in Fig. 3 c, e and f illustrates the extend of the global scour.

lowest node and the sea bed, the flow field around a jacket pile might resemble the one around a cylindrical structure more closely, e.g. if neglecting additional structural elements like post piles. If in contrast the structural contraction of the flow is increased or the distance to the sea bed is reduced, the flow acceleration under the braces rises significantly which has been highlighted by Stahlmann (2013) for a tripod foundation.

Results show, that the scour process and its spatial development around the structure were dependent on the flow condition, i.e. whether the flow was current, or wave dominated. To visualize the influence of the structure on the scouring process, Fig. 3 exemplary presents the scour pattern from wave dominated (U_{cw} = 0.33, test 10) up to steady current conditions (U_{cw} = 1.0, test 13). Wave dominated conditions U_{cw} = 0.33 (U_m = 20.8 cm/s, U_c = 10.11 cm/s) are illustrated in Fig. 3 (a), test 10. A slightly higher wave current velocity ratio of U_{cw} = 0.56 is depicted in test 8, which was conducted under a decreased orbital and increased current velocity (U_m = 17.5 cm/s, U_c = 22.5 cm/s). The bed topography (Fig. 3, b) reveals eroded areas and long-crested sand ripple migration in wave direction with global scour depth of approximately S/D= 0.2–0.4. Fig. 3 (c) and (d) illustrates the bed topography under current dominated conditions U_{cw} = 0.75 (U_m = 13.3 cm/s, U_c = 38.8 cm/s, test 6). Under these conditions, the main direction of sand ripple migration was in line with the current direction. The dashed line, shown in Fig. 3 (c) highlights the extent of global scour with a scour depth of approximately S/D= 0.5–0.6, while the sediment has primary deposited symmetrically, downstream at the sides of the structure. Steady current conditions U_{cw} = 1.0 (test 13), with a flow velocity of U_c = 38.8 cm/s are depicted in Fig. 3 (e) and (f). The lack of the superimposing orbital wave motion results in shorter crested sediment ripples migrating in current direction. The global scour (approx. S/D= 0.6–0.7) is located below and downstream of the jacket and is again highlighted with a dashed line. An explanation of the globally eroded areas (see Fig. 3 c-f) as well as the smaller local scour depth at the downstream side (in current direction) might be the additional influence of near bed wakes coming from upstream located piles and braces.

Enabled by continuous scour depth measurements, infilling of sediment from the edges of the scour hole in combination with a displacement of sediment (backfilling) could be observed for wave-induced, wave-current-induced and current-induced live bed conditions. Driven by the horseshoe vortex as a central element of the scouring process (Sumer and Fredsøe, 2002), an increased scour depth on the upstream side of each pile as well as a decreased scour depth at the downstream side was observed, resulting in an imbalance of scour depth around each pile comparable to that in unidirectional currents (Yao et al., 2016). An increased scour depth under the diagonal braces indicates for an enhanced streamline contraction, and consequently, increased bed shear stresses beneath the braces, similar as shown in Welzel et al. (2019) for a closer distance of the lowest nodes to the sea bed. The observed global scour effects (see Fig. 3) below the structure are further indicators for an altered flow field. Those observations thereby confirm the influence of the structural elements of the complex jacket foundation on the flow field and in turn on the scouring process.

3.2. Scour development under combined waves and current

Fig. 4 illustrates the time dependent scour development of test 4–6 by comparing the scour depth at individual positions around pile 1 and pile 3. Echo sounder E1 – E3 were located around pile 1 (see Fig. 2) at 315° (E1), 45° (E2) and 135° (E3). Here, the structure is mainly affected due to the local vortex system and less due to neighbouring structural elements. Echo sounder E5–E7 were located around pile 3 (see Fig. 2) at 135° (E5), 225° (E6) and 315° (E7). At this location, wave and current induced flows were influenced by the presence of structural elements located on the upstream side of the structure. Unaffected by local scour around the piles, echo sounder E4 and E8 provided pointwise measurements of the global scour depth over time as a reference. Over the course of the tests, scour depths at E4 and E8 were slowly but steadily increasing, and thereby, indicating a positive correlation between U_{cw} and globally occurring sediment transport. As expected, the local scour depths at pile 1 and 3 increased immediately with every step-wise increase of current flow velocity, and subsequently, followed an asymptotical growth towards an equilibrium stage. The increase of current flow velocity between test 4 and 6 was accompanied by an increase of ripple formation and migration. As shown in Fig. 4, the upstream located echo sounder E4 measured in test 4 and 5 larger scour depths, whereas test 6 clearly showed a deeper scour for location E8 on the downstream side. Possible reasons for this are discussed in detail in chapter 3.4.

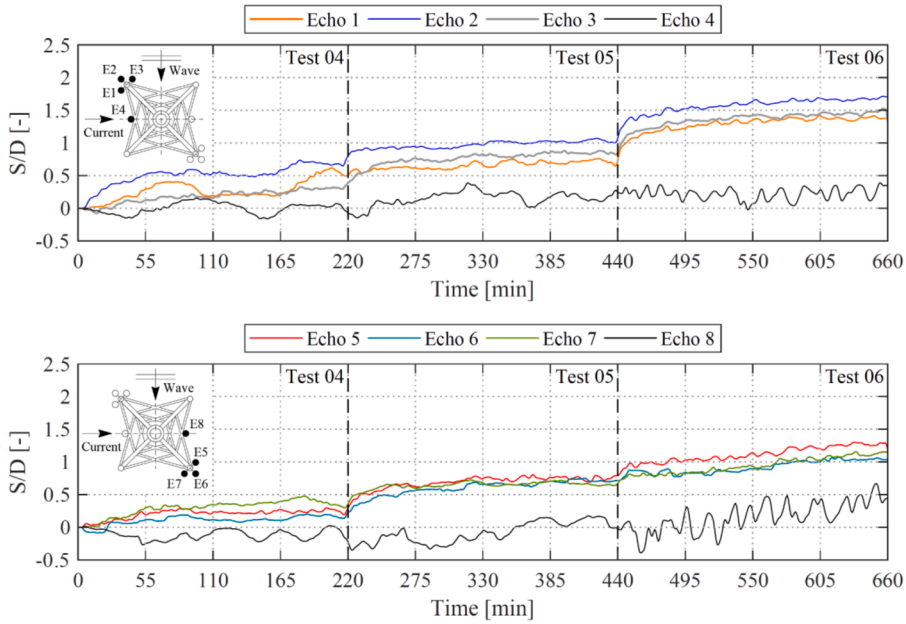

Fig. 4. Test 4–6: Scour progression for KC = 6.7 for positions, referring to Fig. 2, under a near bed current velocity of U_c = 10.1, 22.5 and 38.8 cm/s as well as an orbital velocity of U_m = 13.3 cm/s.

The scouring process at pile 1 was characterised by an imbalance of scour depth between the measurement positions E1-E3, similar to that in unidirectional currents (Yao et al., 2016). In comparison, the differences in scour depth between E5-E7 located at pile 3 were less pronounced. In particular, the distinct differences of scour depths between E2 and E3 indicate a more current dominated scouring process at the upstream pile 1 than at the downstream located pile 3, where the approaching current was partially influenced by pile 4. The structural elements of pile 4 induced additional vortices, which affected the flow acting on the scour development around the downstream located pile 3.

Moreover, a closer look at the scour development at pile 1 also reveals a large difference in scour depth between positions E1 and E2, especially during test 05 and 06, although both echo sounders were located at the upstream side of the pile.

While the scour depth at position E3 was generally smaller than that at position E2, as expected, it was larger than at position E1, which might be explained with slightly increased velocities as pointed out in Miles et al. (2017) at angles of 135° and 225° as well as the impact of flow acceleration due to the crosswise braces. However, the differences between position E1 and E3 diminished with increasing current flow velocity as shown in Fig. 4. For larger values of KC, the imbalance of scour depths around pile 1 were less pronounced than during test 4–6. Test 7–12 (KC = 14.9 & 23.4) showed smaller scour depths for position E3 and higher scour depths for position E1 and E2, which is reasonable, as E3 was sheltered from the current. For the scour development around pile 1 it can therefore be concluded that the scour depths are generally larger at the upstream side, position E1 and E2, than at the downstream side at position E3. While the maximum scour depth remained at position E2 during the tests presented in Fig. 4 (test 4–6), its position varied between E1 and E2 in test 7–9 and remained at position E1 during the course of test 10–12, in which the wave load was further increased to a value of KC = 23.4. Therefore, a clear trend for the position of the maximum scour depth between echo sounder E1 – E3 could not be observed for test 4–12. For the scour development at pile 3 it was found that the position of the maximum scour depth changed from the upstream position E7 in test 4 to the downstream position E5 in test 5 and 6. The transition of maximum scour depth to position E5 might be explained by an increased influence of streamline contraction on the scouring process in test 5 and 6. Due to a higher current velocity, the effect of the streamline contraction should be more pronounced, as the exerted bed shear stresses are increasing proportional to the square of flow velocities. In line with the scour depths at pile 1, maximum scour depth at pile 3 also constantly developed at the upstream side of the pile, i.e. at position E7, during tests with larger wave load and $KC \geq 14.9$.

To account for the described scour depth imbalance between individual measurement positions, the scour depths are given as mean values, averaged over the three measurement positions of pile 1 (E1-E3) and pile 3 (E5-E7) in the following. This procedure is line with several other studies, e.g. Sumer and Fredsøe (2001).

The scour depth fluctuations during test 4 indicate that an equilibrium state was not reached, despite a test duration of approx. 220 min (6 500 waves). Especially echo sounder E1, E2 and E7, located at the upstream side of the piles, showed significant variations of scour depth over time. A possible explanation for these fluctuations might be given by the small erosive potential provided by the combined flow in test 4. With a current flow intensity of only $\bar{U}/U_{crit}$ = 0.39 (U_{crit}= 0.295, calculated with the approach of Melville (1997)), the current alone was not strong enough to maintain a consistent horseshoe vortex and to generate significant scour on the upstream side of the piles. As suggested by Breusers et al. (1997), a flow velocity larger than half of its critical value is required to initiate the scouring process at a pile. In addition, the thickness of the wave boundary layer in the tests can be expected to be relatively thin, potentially too thin to generate a strong horseshoe vortex at the upstream side of the pile so that the lee wake vortices were the major driving forces for the scour development. The steady scour development of test 5 indicates that an increased current velocity (on U_c = 22.5 cm/s) leads to a less fluctuating scouring process. In this current dominated regime, a consistent horseshoe vortex can form that provides a constant erosive potential.

As mentioned earlier, the equilibrium scour depth was not reached in all tests. For current induced scour development in clear-water conditions, Melville and Chiew (1999) as well as Sheppard et al. (2004) reported that it might be necessary to conduct experiments for several days to reach equilibrium conditions. The outcome showed a strong correlation between the estimated time to reach the equilibrium stage and the pile diameter. Consequently, tests with small pile diameters reached the equilibrium condition comparable faster. Qi and Gao (2014) described that the rate of scour depth development under combined waves and current conditions is remarkably faster than in current alone cases. However, their test durations were limited to approx. 100 min, and thus, potentially insufficient to assess the equilibrium scour depth. Therefore, an extrapolation to expected equilibrium scour depths was attempted, as described below. An approach similar to Sheppard et al. (2004) was used to describe the expected time dependent scour development under combined wave-current conditions for the present study:

$$S(t) = a\left(1 - \frac{1}{1 + bt}\right) \tag{4}$$

Eq. (4) was given the preference over the approach of Sheppard et al. (2004) as the latter tended to produce unreliable results with a high degree of uncertainty for tests with strongly fluctuating scour depths. The approach of Sheppard et al. (2004) was defined for current-only conditions with less fluctuating progressions of scour depth over time. The coefficients a and b of Eq. (4) were determined for each test by least square fitting to the measured data. Once the coefficients a and b have been found, time t was increased until the scour depth reached the equilibrium stage without any further increase of scour depth. Exemplarily, Fig. 5 shows the extrapolation to equilibrium scour depth with Eq. (4) for test 10 (measured scour depths are averaged over E1-E3). In Fig. 5, the parameter S_{end} is defined as the mean values of scour depths measured during the last 25% of each test.

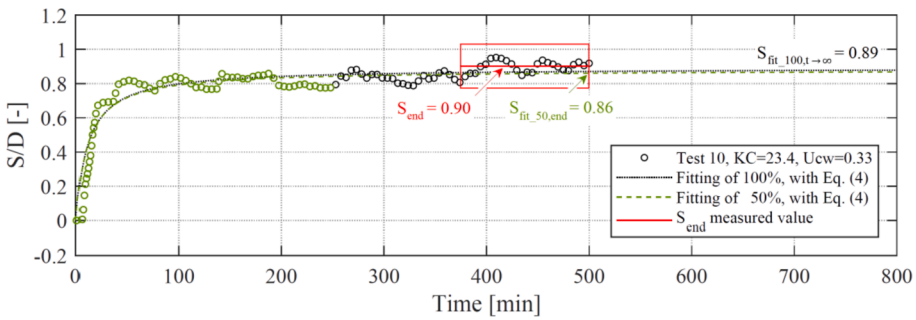

Fig. 5. Extrapolation of measured scour depth to equilibrium scour depth $S_{fit\_100,t\rightarrow\infty}$ for test 10 based on Eq. (4), S_{end} (average value of last 25% of measured scour depth), fitting of 50% of the signal to the end of the test $S_{fit\_50,end}$.

In addition, an uncertainty estimate has been made regarding the performance of the extrapolation to predict the equilibrium scour depth. Therefore, Eq. (4) was applied on only half of the time series, as shown in Fig. 5. Then, the extrapolated scour depth $S_{fit\_50,\,end}$ was compared to the actual measured scour depth at the end of the test. The example, shown in Fig. 5, test 10 reveals a difference between S_{end} and $S_{fit\_50,\,end}$ of 5% ($S_{end}/S_{fit\_50,end} = 1.05$). Overall, the uncertainty analyses with extrapolation based on 50% of the signal revealed an average difference between S_{end} and $S_{fit\_50,end}$ of 18.6%. Without test 6, 9 and 12, the average difference between S_{end} and $S_{fit\_50,end}$ is calculated to 8.7%. Test 6, 9 and 12 revealed larger differences, which can be explained with the influence of the global scour on the local scour development, which in turn affects the extrapolation.

It has to be noted that the following analysis in the present paper is using only measured values (see Table 1, S_{end}). The presented extrapolation analysis is used to critically assess the measured scour depth. Similar as conducted in Sheppard et al. (2004), measured values S_{end} are compared with a value of 90% of the equilibrium scour depths $S_{fit\_100,t\to\infty}$ to assess whether the test reached an equilibrium stage or not. A comparison between 90% of the extrapolated equilibrium scour depths and the measured scour depth S_{end} indicates that, apart from test 6, 9, 12 and 13 (influence due to global scour around pile 3), in particular test 4 (77% of $S_{fit\_100,t\to\infty}$, pile 1 & 3) and test 13 (79% of $S_{fit\_100,t\to\infty}$, pile 1) have not reached the extrapolated equilibrium scour depths value (see Table 1).

To assess the dependency of the scouring process on the KC number, Fig. 6 contrasts the progression of mean scour depth over time at pile 1 and pile 3 for tests with similar values of U_{cw} but different KC numbers. As it was intended to keep the number of waves between tests comparable, the test duration varied between 220 min for tests with $KC = 6.7$ and 500 min for tests with $KC = 23.4$. Thus, the time in Fig. 6 is given as nondimensional time t/t_{end}. The scour depth S is either normalized with the main pile diameter D (4 cm) or with the final scour depth S_{end} of each test to provide a better understanding of influences in the scour development under different load configurations. Furthermore, the illustration of scour development over time as S/S_{end} allows an easier comparison of scouring rates and time scales as shown in the following chapter 3.3.

For a small current load (Fig. 6 (a) and (d)), i.e. in a wave dominated regime, the increase of scour depth as well as the scouring rate correlated positively with the increasing KC number. At both piles, the scour progression induced by $KC = 6.7$ was significantly slower and less asymptotical than that for larger KC numbers. Furthermore, the initiation of the scour process at pile 3 seemed to be delayed for $KC = 6.7$ compared to that at pile 1. This effect might be a result of the aforementioned small erosive potential of test 04 in combination with the time which is necessary to stabilize the vortex shedding around pile 3. With an increasing U_{cw} parameter the scour process became more current dominated, and scour depths were increasing with a similar rate, independently from the KC number. In all tests, the scour progression clearly resembled that in unidirectional currents, showing a steady increase towards an equilibrium scour depth.

During tests with $U_{cw}\geq 0.65$, in particular in test 9 and 12 (pile 1), global scouring processes and dune migration led to an unsteady progression of scour depth over time. To account for these effects on the scour depths, S_{end} is defined as the scour depth at the inflection point in test 9 and 12 (pile 1), instead of using the last 25% of measured scour depths to calculate S_{end}. The inflection point was determined by

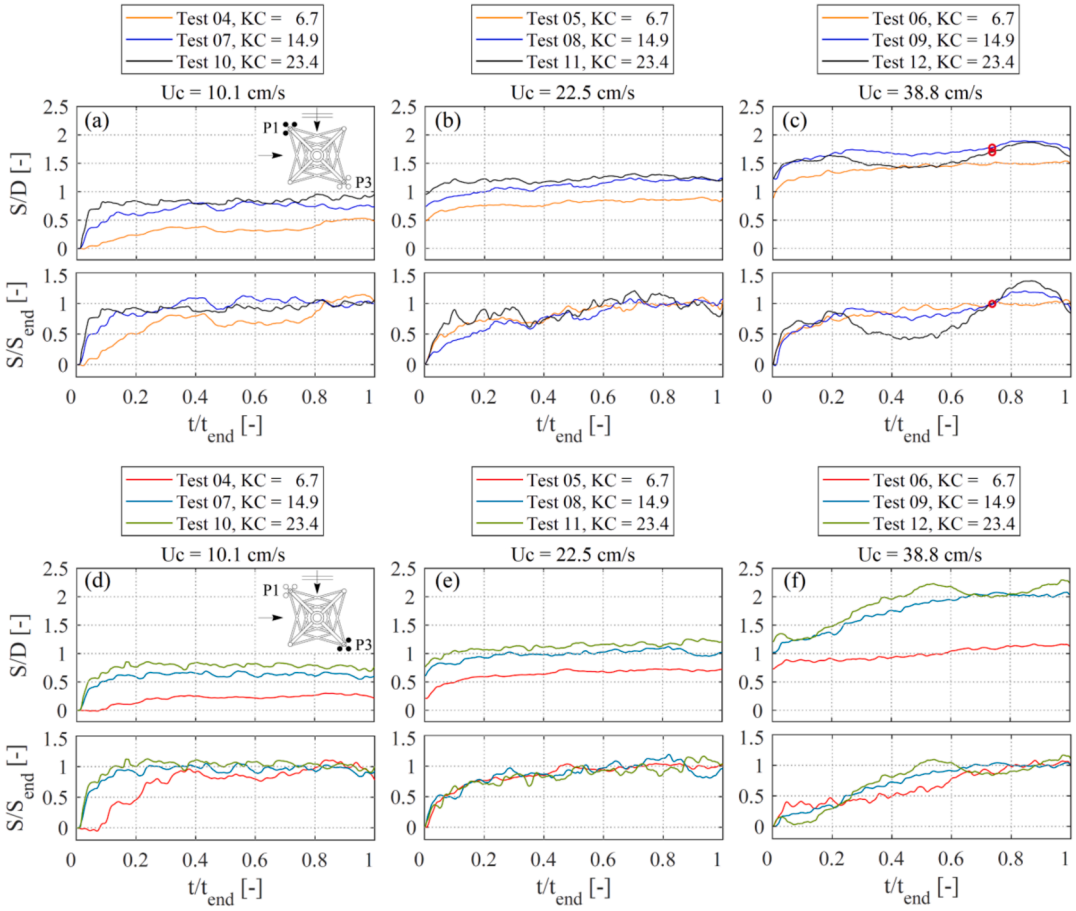

Fig. 6. Scour progression of test 4–12, pile 1 (a–c) and pile 3 (d–f) normalized with the pile diameter (D = 4 cm), the final scour depth value S_{end} plotted over the dimensionless time t/t_{end} as well as the calculated inflection point (red dot) for test 9 and 12.

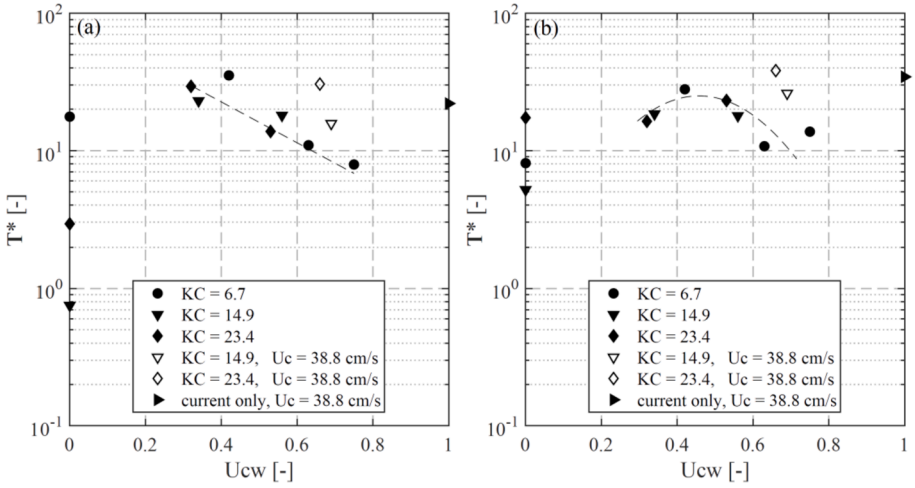

Fig. 7. Nondimensional time scale T^* against U_{cw} for (a) the scour development around pile 1 and for (b) the scour development around pile 3. Dashed lines represent regression curves.

calculating the derivative of the time dependent scour depth measurements and resembles a point during the advanced stage of the test at which the scouring rate reaches a maximum. Furthermore, in the wave only test 2 and 3 a deposition of sand around the structure was observed. In order to complement the test condition matrix and yield comparative understanding to the combined waves and currents experiments those measurements are included in the following timescale and final scour depth analysis. The scour depth of those tests (2 & 3) is taken as a reference to the increased global sea bed level measured with E4 and E8.

3.3. Timescale

The time scale is defined as an additional reference value to assess the scouring rate and is calculated for all tests. Sumer et al. (1992a) defined the time scale as the time which is needed to reach a scour depth of 63% of the equilibrium depth, by applying a tangent to scour development at $t = 0$. As all tests have been conducted in live-bed conditions, the scour development was influenced by sediment infilling, which resulted in an unsteady increase of scour depths. Therefore, as an approach that can take a fluctuating scour development into account, the dimensionless time scale T^* is calculated by integrating the scour depth over the considered time period of the test, similar to the approach applied by Fredsøe et al. (1992), Fuhrman et al. (2014) or Schendel et al. (2018):

$$T^* = \int_0^{t^*_{max}} \frac{S_{max} - S(t^*)}{S_{max}} dt^* \tag{5}$$

in which S_{max} is the maximum scour depth and t^* is the dimensionless time given by:

$$t^* = \frac{(g((s-1)d_{50}^3))^{1/2}}{D^2} t \tag{6}$$

The time scales for the scour development at pile 1 and 3 are summarized in Table 1. During some tests, the scour depth reached an interim maximum, which was slightly larger than the final scour depth at the end of the test. To provide consistency between tests, the maximum scour depth S_{max} as well as the time t^*_{max} at which the maximum scour depth occurs are chosen to calculate the time scale instead of using the final scour depth S_{end}. Considering a monotonically growing scour development curve with less fluctuations, it could be deduced that a calculation of the time scale with eq. (5) and S_{end} instead of S_{max} would lead to an increased time scale value. However, the analysis of the present dataset with a reference on S_{max} revealed similar magnitudes as a calculation with S_{end}, but with a much less pronounced fluctuation of T^*. Since eq. (5) is formulated to represent the area underneath the curve in between t = 0 and t = t_{max}, it is less depending on fluctuations, as fluctuating areas below S_{max} and after t_{max} are not considered. In consequence, the above-mentioned method (relating on S_{max}, see eq. (5)), which was already formulated and formally proven by Fuhrman et al. (2014) is considered to be more reliable for the present study. In Fig. 7, the calculated time scale is presented versus the wave-current velocity ratio U_{cw}, for the scour development of pile 1 (Fig. 7 (a)) as well as for pile 3 (Fig. 7 (b)). As mentioned before, the scour development in test 9 and 12 was influenced by migrating sand dunes. As a result, the calculated time scales for these tests are assumed to be larger than a comparable scour development without the fluctuating influence. Therefore, the time scales of these tests are highlighted separately in Fig. 7, and were not considered for the regression curves shown in Fig. 7. Generally, the nondimensional time scale is decreasing with an increase of U_{cw}, indicating a faster scour progression for larger values of U_{cw}. Furthermore, Fig. 7 (a) reveals that the time scale was more dependent on U_{cw} in tests with small KC numbers (test 4–6) than in those with large KC numbers. As the drag component of the waves become more dominant with increasing KC number the influence of the current on the scouring process is diminishing.

Regarding the temporal evolution of the scour development, it was observed that the local erosion around vertical piles progressed more rapidly than the globally occurring erosion around and underneath the structure. This observation is in agreement with investigations of Stahlmann (2013) on the scour development around a tripod foundation, in which the local scour development at the piles also progressed faster than the global scour development underneath the structure. Furthermore, in contrast to studies by Schendel (2018) or by Petersen et al. (2012), the present study reveals a larger time scale value for current only conditions ($U_{cw} = 1$) in comparison to that in current dominated conditions ($U_{cw} \gtrsim 0.7$). The calculated time scales of pile 1 and 3 indicate that even small orbital velocity components have a significant influence on the present scouring rate. A possible explanation might be the mutual influence and entwined feedback mechanisms between local and global scouring processes, but which are evidently governed by different time scales, related to current dominated or current only conditions.

The comparison of time scales for pile 1 and pile 3 exposes a different dependency of time scales to U_{cw} (see Fig. 7). For values of $U_{cw} > 0.52$ the time scales at pile 3 show a stronger dependency to U_{cw} than those at pile 1. In addition, time scales are larger than those at pile 1 for this range of U_{cw}, implying a slower scouring process at the downstream located pile 3. Reasons for this might include a decreased

influence of the current on the scouring process around pile 3 due to its sheltered position and the influence of the eroded sediment that is induced by the upstream piles and braces. Consequently, the wake of the upstream located structural elements modifies the incoming flow conditions and the incident vorticity field. The downstream located pile interferes with the wake dynamics and vortex formation of the upstream located piles and braces, rather similar to two circular cylinders in a tandem configuration (Mubeen, 2008; Sumner, 2010). As a result, upstream located structural elements affected the downstream located sediment bed as well as pile 3, leading to global scouring for higher U_{cw} values. The observed scour development of E4 and E8 suggest that global scouring is governed by processes on a different time scale compared to the local scour process around each pile. A comparison of echo sounder E8 with test 6, pile 3 (see Fig. 5), illustrates the influence on the scour development and thus also on the time scale, which was observed for tests with $U_{cw} \geq 0.65$ at pile 3 (Fig. 7, b).

The mobilization of sediment by the upstream piles also increase with increasing current velocity, potentially leading to a significant slowdown of the scouring process at pile 3 especially for higher current loads compared to that at pile 1. On the other hand, for values of $U_{cw} < 0.52$, time scales indicate a faster scour progression around pile 3 than at pile 1. This finding is in accordance with the scour development presented in Fig. 7, which also shows a faster increase of scour depth at pile 3 than at pile 1. In contrast to pile 3, the flow around pile 1 was unaffected by the vorticity field of neighbouring structural elements. A possible explanation for the larger time scales at pile 1 at low U_{cw} values might thus be given by the small erosive potential provided by the current flow at $U_c = 10.1$ cm/s, which in turn leads to a slower scouring rate at pile 1 than at pile 3. Finally, it has to be noted that the determination of time scales could be influenced by the successive load conditions coming with the test procedure.

3.4. Influence of KC and U_{cw}on the final scour depth

Fig. 8 compares the final scour depths S_{end} at pile 1 and pile 3 as a function of KC and U_{cw}. As depicted, the scour depths at the upstream pile 1 and the downstream pile 3 followed the same trend, namely that scour depths increase with increasing KC number. This trend and even the rate of scour depth increase with increasing KC number was generally unaffected by U_{cw}. Only for values of $U_{cw} > 0.65$, and thus in current dominated flow condition, a significant difference between the scour depths at pile 1 and 3 in terms of dependency to KC could be measured. Here, scour depths at pile 3 seemed to be more dependent on the KC number as scour depths at pile 1. As mentioned before, the scour depths in tests with a large current velocity might however be influenced by dune migration. Therefore, test 9 and 12 are excluded for the calculation of the regression curves of pile 3, shown in Figs. 8 and 10. Overall, final scour depths were slightly larger at pile 1 than at pile 3. For values of U_{cw} in the range of 0–0.63, scour depths at pile 3 were on average 0.14 S_{end}/D smaller than those at pile 1.

Additionally, Fig. 9 (a) shows the development of scour depth at both piles with increasing U_{cw}, from a wave to a current dominated flow regime, for all tests. For visual reference, the inner graphical subset in Fig. 9 depicts the position of each echo sounder around the jacket structure. In current dominated conditions, $U_{cw} \rightarrow 1$, scour depths approached values similar to those obtained for current only conditions, whereas in wave dominated situations, $U_{cw} \rightarrow 0$, scour depths close to those in "waves-only" conditions were observed. While scour depths generally increased with KC number over the whole range of U_{cw}, the influence of KC on the scour depths was significantly larger in the wave dominated than in the current dominated regime. As pointed out by Sumer and Fredsøe (2001) for the scour development at monopiles, this indicates that for small KC numbers only a small superimposed current can considerably increase the wave induced scour depths. Following the approach of Sumer and Fredsøe (2001), Eq. (7) is proposed to predict the scour depths at a jacket type foundation structure in combined wave and current flow conditions. As scour depths were found to be significantly different whether the upstream pile 1 or the downstream pile 3 is considered, the prediction of scour depths by Eq. (7) differentiates between both locations. Furthermore, it has to be noted that Eq. (7) is valid for measured scour depths S_{end} of the present study, and for one particular wave-current structure alignment of waves propagating in 90° to the current.

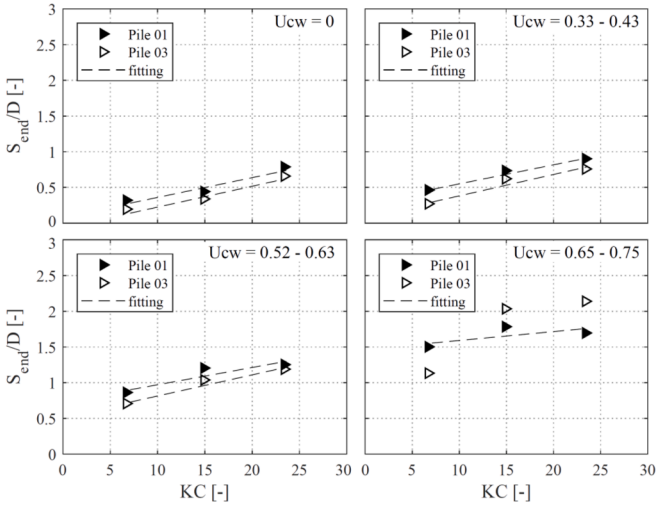

Fig. 8. Measured nondimensional scour depths S_{end}/D, plotted over KC for different U_{cw} wave-current velocity ratios.

$$\frac{S_{end}}{D} = (0.7 + \exp(-6.5\, U_{cw}^{2.5} - A))^{-1.5} + 0.17 \tag{7}$$

with:

$$A_{front} = 1.66\, KC^{0.34} - 4.5 \tag{7a}$$

$$A_{rear} = 1.30\, KC^{0.40} - 4.6 \tag{7b}$$

To evaluate the development of global scour between the individual piles of the jacket structure, Fig. 9 (b) illustrates the final scour depths measured by echo sounder E4 and E8, which were placed in the middle between the upstream and downstream piles (Fig. 2), respectively. As the measurements of E4 and E8 depict point measurements at two distinct locations, no sound statement on the extend of global scour can be derived from them. Nevertheless, they might provide additional information on the ratio between global and local scour at both the upstream and downstream side of the structure (again looking in current direction). As expected, scour depths at the positions of E4 and E8 increased with rising current flow velocity, i.e. increasing values of U_{cw}. However, under wave only conditions a deposition of sediment instead of scour was partly measured. Furthermore, the measurement at E4 and E8 indicate an increasing scour depth with increasing values of KC, especially at the upstream located echo sounder E4. The fitting of scour depths at E4 and E8 indicates that the global scour depth followed a similar trend as the measured local depth around pile 1 and 3. However, the change of the scour depth at location E4 and E8 with U_{cw} was clearly less pronounced than that of the local measured depth. Measurements at locations E4 and E8 did not show a clear equilibrium stage for every test (see Fig. 5, pile 3). The sediment erosion and redistribution in the globally affected areas in between and around the structure's footprint are mainly affected due to wake dynamics and vortex formations as well as streamline contraction induced by the structural geometry of the jacket. This finding indicates that local and global scouring processes are governed by processes on different time scale and are affected by characteristic depth ratio but are correlated to each other by means of entwined feedback mechanisms. The trend line of pointwise global scour measurements (Fig. 9, b; E4 and E8) reveals a

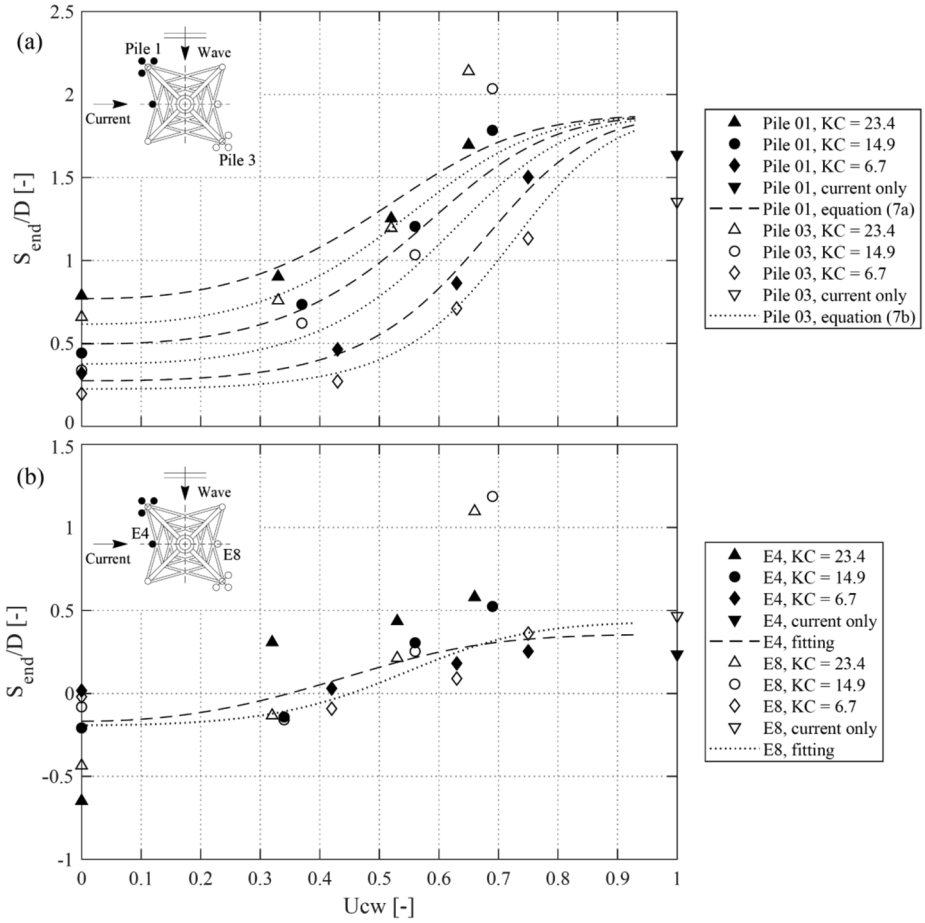

Fig. 9. Measured nondimensional scour depths S_{end}/D versus U_{cw}. S_{end}/D depicts the mean value of echo sounder measurements at pile 1 (E1-E3) or pile 3 (E5-E7).

correlation between the global scour depth and the increase of the wave current velocity ratio U_{cw}. Nevertheless, it cannot be deduced, whether the pointwise echo sounder measurements of E4 and E8 are influenced due to a local scouring effect. As a result, a detailed statement about the fraction of the scour depth, which is attributed to local or global scour cannot be made within the present study.

Scour depths in combined flow conditions are usually smaller than in equivalent current only conditions, at least for the case of a monopile. Here, larger local scour depths were obtained, in particular for test 6, 9 and 12 (Fig. 9, a), potentially due to the influence of the global scour, leading in curves of Eq. (7) ending above the current alone measurement. Furthermore, the extrapolation analysis, shown in paragraph 3.2 revealed that test 13 (current only) did not fully reached the equilibrium stage and thus might be a bit underestimated. The influence of the global scour on local scour development becomes apparent through a comparison of the time dependent scour depth signal at each pile (E1-3, E5-7) with the associated measurement of E4 and E8 (not illustrated), which is rising equally to the local scour depth around the pile for these tests. The two outliers (Fig. 9a and b; pile 3) can be explained, due to the combined effect of global scour and dune migration, which were more pronounced in test 9 and 12.

A comparison between studies of Chen et al. (2014) and Bolle et al. (2012) reveals partly similar as well as deeper scour depths for the present study. However, it has to be noted that both studies measured the scour depth after a comparable short time period. Whereas a comparison with measurements of Rudolph et al. (2004) shows that scour depths of the present study are generally smaller. This might be explained by a significantly increased contraction of the flow due to near bed structural elements of the jacket structures investigated by Rudolph et al. (2004). Furthermore, the sea bed elevation measured in Chen et al. (2014) indicates for a comparable scour mechanism as local and global erosion seemed to dominate on the upstream side of the structure. Similar to measurements of the present study, field measurements of Rudolph et al. (2004) as well as Baelus et al. (2019) reveal a global scour around the jacket foundation. On the other hand, multibeam echo sounder scans of Bolle et al. (2012) did not show a clear global scour but indicate that the erosion process was in an early stage.

3.5. Comparison with scour depths at monopiles

While the findings on the scour development around the jacket structure alone provide already valuable insights in the scour processes around the complex foundation structure, a direct comparison to scour depths at monopiles might additionally allow the definition of application-oriented reference values for an improved prediction of scour at jacket structures.

For this comparison, scour depths measured at the upstream pile 1 of the jacket structure, where the scouring process should have been less affected by the structure than at pile 3, are considered. These scour depths are compared to data obtained by Schendel (2018), who conducted model tests on the scour process around a monopile structure (with a diameter of 8 cm) in combined wave and current conditions. The model tests of Schendel (2018) were carried out in the same facility and under similar hydraulic condition as the tests presented herein, reducing the uncertainties between individual studies stemming from model effects or different test procedures. As further reference for the scour development at a monopile in current only conditions, data from the experimental study of Schendel et al. (2018) were used.

For a comparison of scouring rates, Fig. 10 contrasts the dimensionless time scales of both studies against U_{cw}. Here, the time scales

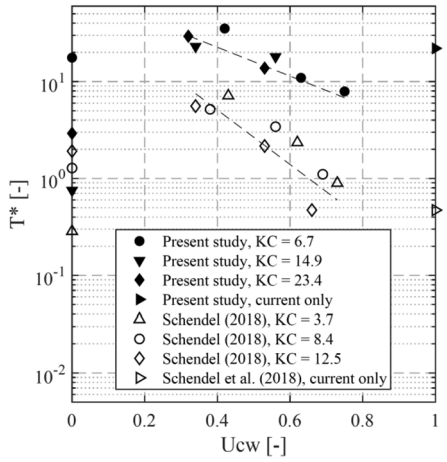

Fig. 10. Nondimensional time scale over U_{cw}, plotted for KC = 6.7, KC = 14.9 and KC = 23.4 in comparison to data of Schendel et al. (2018) and Schendel (2018) for a monopile.

for both studies were calculated following the approach given by Eqs. (5) and (6). In general, it can be summarized that the scour development of the present tests led to slower scouring rates in comparison with the monopile tests of Schendel (2018). While the time scales for the scouring process at both structures decreased with increasing U_{cw}, the magnitude of the decrease was different so that in current dominated flow the final scour depths at the jacket structure developed comparable slower than those at the monopile. Overall, Fig. 10 thus indicates that the scouring process at the investigated jacket structure progressed slower and was also less dependent on U_{cw} than the scouring process at a monopile structure.

In Fig. 11, measured scour depths S_{end} normalized with the pile diameter are plotted against results from Schendel (2018) and Sumer and Fredsøe (2001) as a function of KC and U_{cw}. The tests of Sumer and Fredsøe (2001) have been conducted under comparable conditions regarding the Keulegan Carpenter number, similar to that of the present study. Nevertheless, it has to be noted that tests of Sumer and Fredsøe (2001) related to KC = 8 and 26 have been conducted for codirectionally propagating current and waves, while tests related to KC = 18 were conducted for waves propagating perpendicular to the current.

While some scattering of scour depths is obvious, which is expected given the prevailing uncertainties coming from model and scale effects, the results show a comparable dependency of scour depths on U_{cw} and KC numbers. The scour depths generally increased with KC over the whole range of U_{cw}. The influence of KC on the scour depth was significantly larger in the wave dominated than in the current dominated regime. Nevertheless, it can also be taken from Fig. 11 that the scour depths of Sumer and Fredsøe (2001) were slightly more dependent on the KC numbers than those measured in the present study, for U_{cw} values less then ~0.4. Furthermore, scour depths given by Sumer and Fredsøe (2001) were considerable larger than those presented herein for similar KC numbers and U_{cw} values. The maximum scour depth difference between values of Sumer and Fredsøe (2001) and the present study reached from $\Delta S_{end}/D \approx 0.43$ ($U_{cw} = 0.33$) for KC = 23.4, to $\Delta S_{end}/D \approx 0.32$ ($U_{cw} = 0.56$) for KC = 14.9 as well as up to $\Delta S_{end}/D \approx 0.20$ for $U_{cw} = 0.63$ and KC = 6.7. Differences in terms of scour depths and their dependency on KC and U_{cw} between the present study and Schendel (2018) were less pronounced (see Schendel, 2018, KC = 8.4), which might be partly explained by the fact that the tests of Schendel (2018) were also carried out with a perpendicular superimposition of current and waves. While Sumer and Fredsøe (2001) found no influence of the direction of wave propagation on the scour depth around a monopile, the angle of wave-current superimposition might be more important for the scouring process at a complex jacket structure.

Finally, Fig. 12 evaluates the accuracy of the approach of Sumer and Fredsøe (2002) and of Eq. (7) to predict the scour depths obtained in this study by comparing the measured scour depths of pile 1 and 3 to predicted values. It has to be noted that a good prediction of the present model tests is expected with a comparison of Eq. (7), as Eq. (7) is fitted to these very tests. But the comparison also highlights the difference between Eq. (7) and the approach of Sumer and Fredsøe (2002), defined for monopiles. The approach given by Eq. (7) provides an improved prediction of scour depths ($R^2 = 0.95$) compared to the approach of Sumer and Fredsøe (2002) ($R^2 = 0.58$) for pile 1. Despite of the underprediction of test 9 and test 12 which are considered as outliers as discussed in 3.4, the present approach ($R^2 = 0.87$) provides a good correlation between measured and predicted values compared to

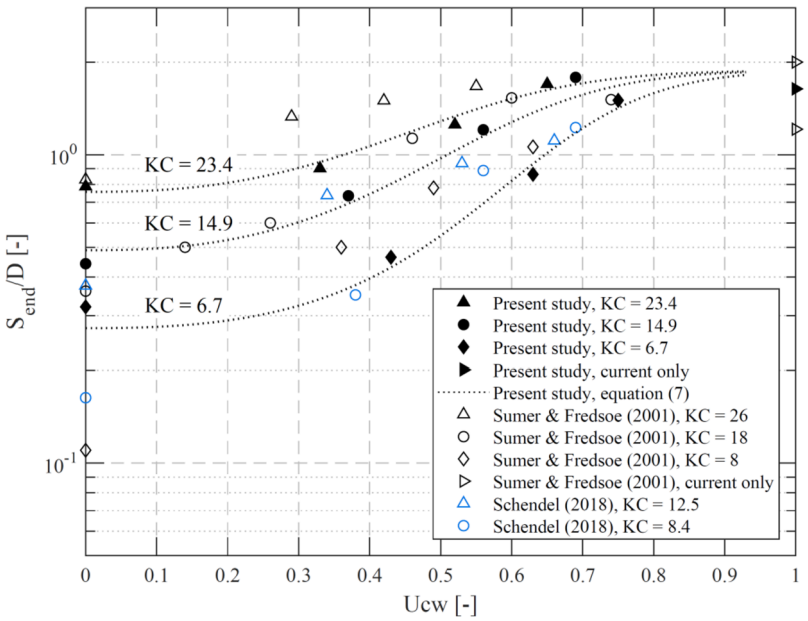

Fig. 11. Measured scour depths for pile 01, $U_{cw} = 0$ indicate Waves alone and $U_{cw} = 1.0$ indicate current alone tests, present data compared with monopile data of Sumer and Fredsøe (2001) and Schendel (2018).

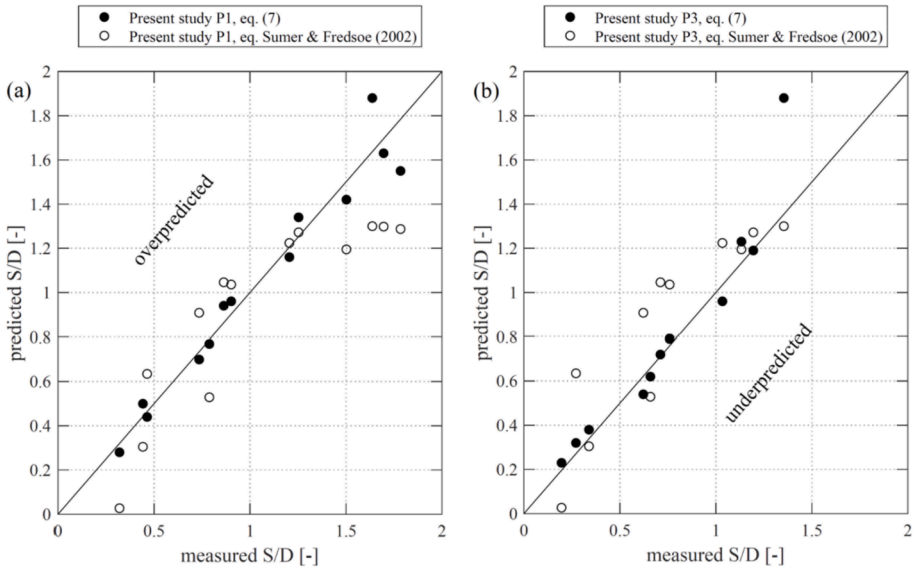

Fig. 12. (a) Over- and underpredicted measurements of pile 1 compared with the prediction formula after Sumer et al. (2002), $R^2 = 0.58$ and formula (7) $R^2 = 0.95$ (b) over- and underpredicted measurements of pile 3 compared with prediction after Sumer et al. (2002), $R^2 = 0.73$ and eq. (7) $R^2 = 0.87$.

the approach of Sumer and Fredsøe (2002) ($R^2 = 0.73$) for pile 3. The approach of Sumer and Fredsøe (2002) tends to underpredict the scour depths measured at pile 1 and tends to overpredict scour depths around pile 3, especially for very small or large values of U_{cw}. This is generally explained by the impact of the complex structure on the surrounding sea bed. A comparison with measurements of echo sounder E4 and E8 indicates that increased measurements with a large U_{cw} value are related to an increase of the global scour (see Fig. 9) as well as the influence of additional near bed structural elements as for example diagonal braces. However, it has to be noted that, only few tests with a low U_{cw} value could be realized during the present study. Further studies are necessary to provide a better understanding of scour depth for low U_{cw} values.

3.6. Remarks regarding the influence of structural elements on the scour depth

The present study was conducted for a jacket structure, with the near bed braces located one pile diameter (1D) above the sediment bed. In relation to previous studies, e.g. Chen et al. (2014), the diameter of the diagonal braces (present study) was comparable large (0.55D, at the nodes 0.73D). In combination with the diagonal braces being close to the sea bed, the jacket structure used in the present study represents a foundation structure with a larger contraction of the flow. Compared to more hydrodynamically transparent structures, a stronger streamline contraction, and thus, increased bed shear stresses might be a result, ultimately leading to an increased scour potential shown in Welzel et al. (2019). However, as shown in Fig. 11, scour depths measured in the present study were on a comparable level with those obtained for monopiles. In contrast, field measurements shown in Rudolph et al. (2004) indicate local scour depths 3–4 times as large as those predicted for a monopile foundation. The jacket structures described by Rudolph et al. (2004) have been installed with additional post piles and were characterised by horizontal and diagonal braces that reached down to the sea bed. Post piles positioned close to main piles might be considered as something similar as a pile group consisting of two circular cylinders with comparable effects on the scour development.

Sumner (2010) summarized and described findings of various studies dealing with the flow around two circular cylinders. He found that the flow around two piles placed at a distance of 1-2D to each other behaves as the flow near a single body or an “extended body”. Furthermore, Sumer and Fredsøe (1998) and Sumer et al. (2001) conducted scouring experiments with groups of piles including two piles close to each other. The results showed that the total scour around two piles can be increased on up to ~1.3 times the single pile scour depth for current conditions, which reveals that additional erosion might come from the combination of a pile group with additional near bed braces as well as the additional influence of global scour on the local scour development to reach values $> 3\ S/D$.

At this point, to provide any form of guidance towards a scour reducing jacket design, the following assumptions could be made with regard to the general influence of individual structural elements on the scour development. First, local scour depths are significantly increased by additional post pile. Furthermore, the smaller the distance between horizontal or diagonal braces and the sea bed, the larger scour depths can be expected. Finally, reducing the distance between the main piles or increasing the diameter of the braces will lead to an increased contraction of the flow and potentially larger scour depth. As it has been demonstrated by the findings of this study, the scouring process, in particular the globally occurring sediment displacement processes, can differ significantly from that around at a cylindrical monopile structure. However, to fully understand the contribution of individual structural elements on the holistic scouring process at jacket structures future studies should strive towards a systematically investigation by an incremental change of structural features. Furthermore, a more focused study related to the time scale and influence of global scour on the local scour development seems to be necessary to gain a deeper understanding of the complex scouring mechanism around jacket structures.

4. Summary and conclusion

Hydraulic model tests were carried out to investigate the scouring process around a jacket-type offshore foundation in combined waves and current conditions. Additional wave and current only experiments have been conducted in order to yield comparative understanding for a wide range of U_{cw} and KC values. Experiments were conducted with irregular wave spectra which propagated perpendicular to a superimposed current. Continuous scour depths measurements with a high temporal resolution have been performed by means of an echo sounding system consisting of eight devices with a diameter of 1 cm, respectively. Novel insights into the intrinsic development of scour around a complex jacket structure were presented. The findings of the present study might thus help to improve the assessment of the scouring process around jacket structures in marine conditions as part of the design process of offshore structures.

The main conclusions can be summarized as follows:

- Jacket structures are often referred to as hydrodynamical transparent structures. While this might be true regarding the influence on the wave field, the flow vortex system and consequently the morphodynamics around the structure are clearly affected by the structure's elements as shown in this study. The influence of the structure results in a flow acceleration between the individual piles and in a more complex vortex system than that around a single pile, in particular in combined wave and current conditions. Consequently, the scour pattern around the jacket structure was characterised by a combination of local scour at the piles and global scour underneath and around the structure's footprint.
- Infilling of sediment from the edges of the local scour holes in combination with a displacement of sediment resulted in a significant variation of the scour development curve, leading to an altering position of the maximum scour depth over time. In general, the experiments showed larger scour depths at the upstream side of the main piles than at the downstream side with respect to the current flow direction. However, this imbalance of scour depth was more pronounced at the upstream pile 1 than at the downstream pile 3, potentially indicating a more current dominated scouring process at the former. Furthermore, an increased scour depth under the diagonal braces, was observed after the tests, which indicates an increased contraction of the flow, and consequently an increased bed shear stress due to the streamline contraction under the braces.
- Unaffected by local scour around the piles, two additional echo sounders measured the global scour depth pointwise. The measurements show an increasing global scour depth with an increasing wave current velocity ratio U_{cw}. Scour depths at location E4 and E8 are around 83% ($U_{cw} = 0.55$) up to 80% ($U_{cw} = 0.75$) smaller than those directly at the piles. The present study demonstrates that scour is developing faster around a jacket structure under combined wave-current conditions than under steady current conditions. The scour development and time scale are found to be different for a pile which is directly exposed to combined waves and current (pile 1) in comparison to a pile which is affected due to neighbouring structural elements (pile 3). While scour depths around pile 3 have been found to be smaller than at the upstream side (pile 1), a slower scour progression for $U_{cw} > 0.52$ and a faster for $U_{cw} < 0.52$ was observed on the downstream side (pile 3) in comparison to pile 1.
- A comparison of dimensionless time scales with values of Schendel (2018) shows a slower scouring rate at the jacket structure than at a monopile, if the diameter of the main piles is used for normalization of the time scale. Additionally, the comparison reveals a different dependency of scour depths to U_{cw}, as time scale is decreasing in a flatter trend, leading to comparable slower scouring rates for current dominated conditions than those at the monopile.
- The final scour depth around an upstream and downstream located pile is a function of the wave current velocity ratio and of the Keulegan-Carpenter number. Accordingly, an empirical expression for the prediction of scour depths at a jacket structure in combined wave current conditions is proposed, which also differentiates between the scour development at an upstream and downstream located pile of the jacket structure.

Acknowledgements

The authors gratefully acknowledge the support of the German Federal Ministry for Economic Affairs and Energy within the funded project “HyConCast – Hybrid substructure of high strength concrete and ductile iron castings for offshore wind turbines” (BMWI: 0325651A). Furthermore, the authors thank T. Kreklow, O. Fink, N. Ommen and L. Evers for their support in conducting the laboratory experiments.

Notation

a, b	curve fit coefficients relating to eq. (4)
D	pile Diameter of the main struts of the jacket structure
d_{16}	grain size for which 16% of the material by weight is finer
d_{50}	grain size for which 50% of the material by weight is finer
d_{84}	grain size for which 84% of the material by weight is finer
f	Frequency
g	gravitational acceleration
H_s	significant wave height
KC	Keulegan-Carpenter number
R^2	Coefficient of determination
s	specific density of the sand
S	Scour depth
$S(f)$	Velocity frequency spectrum
S_{end}	Mean value of the last 25% of the measured scour depth
S_{eq}	Extrapolated equilibrium scour depth
S_{max}	Maximum scour depth
$S(t)$	time dependent scour depth value
t	time in seconds
t^*	dimensionless time corresponding to eqs. (5) and (6)
t_{end}	corresponding time to S_{end}
T^*	dimensionless time scale
U	orbital velocity at the bed in direction of the waves
U_c	undisturbed current velocity at 2.5D from bed
$\bar{U}$	mean current velocity of the vertical profile
U_{cw}	wave-current velocity ratio $U_{cw} = U_c/(U_c + U_m)$
U_m	undisturbed maximum orbital velocity at 2.5D from bed
U_{rms}	root-mean-square (RMS) value U of at the seabed
θ	Shields parameter
θ_{cr}	critical value of the Shields parameter
ν	viscosity of water
σ_g	geometric standard deviation

References

Baelus, L., Bolle, A., Szengel, V., 2019. Long term scour monitoring around offshore jacket foundations on a sandy seabed. In: Ninth International Conference on Scour and Erosion, ICSE 9. 5.-8. November 2018, Taipei, Taiwan.
Baykal, C., Sumer, B.M., Fuhrman, D.R., Jacobsen, N.G., Fredsøe, J., 2017. Numerical simulation of scour and backfilling processes around a circular pile in waves. Coast. Eng. 122, 87–107.
Bolle, A., de Winter, J., Goossens, W., Haerens, P., Dewaele, G., 2012. Scour monitoring around offshore jackets and gravity based foundations. In: Sixth International Conference on Scour and Erosion, ICSE 6. 27.-31. August 2012 in Paris.
Breusers, H.N.C., 1972. Local Scour Near Offshore Structures, vol. 105 Delft Hydraulics Publication, Delft.
Breusers, H.N.C., Nicollet, G., Shen, H.W., 1977. Local scour around cylindrical piles. J. Hydr. Res., Delft, The Netherlands 15 (3), 211–252.
Chen, H.H., Yang, R.Y., Hwung, H.H., 2014. Study of hard and soft countermeasures for protection of the jacket-type offshore wind turbine foundation. J. Mar. Sci. Eng. 2, 551–567 2014.
Fredsøe, J., Sumer, B.M., Arnskov, M.M., 1992. Time scale for wave/current scour below pipelines. Int. J. Offshore Polar Eng. 2 (2), 13–17.
Fuhrman, D.R., Baykal, C., Sumer, B.M., Jacobsen, N.G., Fredsøe, J., 2014. Numerical simulation of wave-induced scour and backfilling processes beneath submarine pipelines. Coast. Eng. 94, 10–22.
Hirai, S., Kuruta, K., 1982. Scour Around Multiple- and Submerged Circular Cylinders, vol. 23. Memoirs Faculty of Engineering, Osaka City University, pp. 183–190.
Hjorth, P., 1975. Studies on the Nature of Local Scour. Bull. Series A, No. 46. Dept. of Water Resour. Engrg., Lund Inst. of Technol., University of Lund, Lund, Sweden.
Kobayashi, T., Oda, K., 1994. Experimental study on developing process of local scour around a vertical cylinder. Chapter 93. In: Proc., 24th Int. Conf. On Coast. Engrg., vol. 2. pp. 1284–1297.
Mansard, E., Funke, E., 1980. The measurement of incident and reflected spectra using a least squares method. In: Proceedings, 17th International Conference on Coastal Engineering, vol. 1. pp. 154–172 (Sydney, Australia).
McGovern, D.J., Ilic, S., Folkard, A.M., McLelland, S.J., 2014. Time development of scour around a cylinder in simulated tidal currents. J. Hydraul. Eng. 140 (6).
Melville, B.W., 1997. Pier and Abutment Scour: Integrated Approach. J. Hydraul. Eng 123, 125–136.
Melville, B.W., Coleman, S.E., 2000. Bridge Scour. Water Resources Publications, CO.
Melville, B.W., Chiew, Y.M., 1999. Time scale for local scour in bridge piers. J. Hydraul. Eng. 125, 59–65.
Miles, J., Martin, T., Goddard, L., 2017. Current and wave effects around windfarm

monopile foundations. Coast Eng. 121, 167–178.
Mubeen, B., 2008. Effect of Mutual Interference of Bridge Piers on Local Scour, PhD Thesis. Department of Civil Engineering, Aligarh Muslim University, Aligarh, India.
Petersen, T.U., Sumer, B.M., Fredsøe, J., 2012. Time scale of scour around pile in combined waves and current. In: Sixth International Conference on Scour and Erosion, ICSE 6. 27.-31. August 2012 in Paris.
Qi, W.G., Gao, F.P., 2014. Physical modeling of local scour development around a large-diameter monopile in combined waves and current. Coast Eng. 83, 72–81.
Raaijmakers, T., Rudolph, D., 2008. Time-dependent scour development under combined current and waves conditions – laboratory experiments with online monitoring technique. In: Fourth International Conference on Scour and Erosion, ICSE 4. 5.-7. November 2008 in Tokyo, Japan.
Raudkivi, A.J., 1986. Functional trends of scour at bridge piers. J. Hydr. Engrg., ASCE 112 (1), 1–13.
Rudolph, D., Bos, K.J., Luijendijk, A.P., Rietema, K., Out, J.M.M., 2004. Scour around offshore structures – analysis of field measurements. In: Second International Conference on Scour and Erosion, ICSE 2. 14.-17. November 2004 in Singapore.
Rudolph, D., Bos, K.J., 2006. Scour around a monopile under combined wave current conditions and low KC-numbers. In: Third International Conference on Scour and Erosion, ICSE 3. 01.-03. November 2006 in Amsterdam, The Netherlands.
Schendel, A., 2018. Wave-current-induced Scouring Processes and Protection by Widely Graded Material. PhD. Thesis Leibniz University Hannover, Germany. https://doi.org/10.15488/4453.
Schendel, A., Hildebrandt, A., Goseberg, N., Schlurmann, T., 2018. Processes and evolution of scour around a monopile induced by tidal currents. Coast Eng. 139, 65–84. https://doi.org/10.1016/j.coastaleng.2018.05.004.
Sheppard, D.M., Odeh, M., Glasser, T., 2004. Large scale clear-water local pier scour experiments. J. Hydraul. Eng. 130, 957–963.
Sheppard, D.M., Miller, W., 2006. Live-bed local pier scour experiments. J. Hydraul. Eng. 132 (7), 635–642.
Stahlmann, A., Schlurmann, T., 2010. Physical modeling of scour around tripod foundation structures for offshore wind energy converters. Proceedings of the International Conference on Coastal Engineering 32, 1–12 Shanghai, China.
Stahlmann, A., 2013. Experimental and Numerical Modeling of Scour at Offshore Wind Turbines. PhD. Thesis. Leibniz University, Hannover, Germany.
Soulsby, R., 1997. Dynamics of Marine Sands: A Manual for Practical Applications. Thomas Telford, London (UK).
Soulsby, R., Clarke, S., 2005. Bed Shear-Stresses under Combined Waves and Currents on Smooth and Rough Beds. Report TR 137 Rev 1.0 August 2005 HR Wallingford.
Sumner, D., 2010. Two circular cylinders in cross-flow: a review. J. Fluids Struct. 26, 849–899.
Sumer, B.M., Christiansen, N., Fredsøe, J., 1992a. Time scale of scour around vertical pile. In: Proc., 2nd Int. Offshore and Polar Engrg. Conf., vol. 3. International Society of Offshore and Polar Engineers, San Francisco, Calif, pp. 308–315.
Sumer, B.M., Fredsøe, J., Christiansen, N., 1992b. Scour around a vertical pile in waves. J. Wtrwy., Port, Coast., and Oc. Engrg. 118 (1), 15–31 ASCE.
Sumer, B.M., Christiansen, N., Fredsøe, J., 1997. The horseshoe vortex and vortex shedding around a vertical wall-mounted cylinder exposed to waves. J. Fluid Mech. 332, 41–70.
Sumer, B.M., Fredsøe, J., 1998. Wave scour around group of vertical piles. J. Waterw. Port, Coast. Ocean Eng. 124 (5), 248–256.
Sumer, B.M., Fredsøe, J., 2001. Scour around pile in combined waves and current. J. Hydraul. Eng. 127, 403–411.
Sumer, B.M., Whitehouse, R.J.S., Tørum, A., 2001. Scour around coastal structures: a summary of recent research. Coast Eng. 44, 153–190.
Sumer, B.M., Fredsøe, J., 2002. The Mechanics of Scour in the Marine Environment. World Scientific, New Jersey, Singapore, London, Hong Kong.
Sumer, B.M., Petersen, T.U., Locatelli, L., Fredsøe, J., Musumeci, R.E., Foti, E., Waterway, J., Port, Coastal, 2013. Backfilling of a scour hole around a pile in waves and current. Ocean Eng. 139, 9–23.
Sun, X., Huang, D., Wu, G., 2012. The Current State of Offshore Wind Energy Technology Development. Elsevier journal, energy, pp. 298–312.
Welzel, M., Schlurmann, T., Hildebrandt, A., 2019. Local scour development and global sediment redistribution around a jacket-structure in combined waves and current. Ninth International Conference on Scour and Erosion, ICSE 9, 5–8 November 2018, Taipei, Taiwan.
Yao, W., An, H., Draper, S., Cheng, L., Zhao, M., Jesudoss, J.S., Tang, G., 2016. Experimental study of local scour around piles in tidal currents. In: Proc. 20th Australasian Fluid Mechanics Conference, Perth, Australia.
Zanke, U.C.E., Hsu, T.W., Roland, A., Oscar, L., Reda, D., 2011. Equilibrium scour depths around piles in noncohesive sediments under currents and waves. Coast. Eng. 58, 986–991.